A Mathematical Model of Slag and Metal Flow in the ESR Process

A. H. DILAWARI AND J. SZEKELY

Through the statement of the turbulent Navier-Stokes equations and Maxwell's equations a mathematical representation is developed for the electromagnetic force field and the velocity field in the slag phase and the metal pool of cylindrical ESR units. Computed results are presented for both industrial scale (0.5 m electrode diameter) and laboratory scale (0.05 m electrode diameter) units operating with direct currents. It was found that for industrial scale units, the computed slag velocities ranged from 5 to 10 cm/s, while the velocities in the metal pool were substantially lower, except at the slag-metal interface. At a given spatial position, the velocity was found to increase in an almost linear fashion with the current density. The flow was found to be predominately laminar in the laboratory scale units and for comparable current densities the melt velocities were very much smaller. Some 600 to 900 s were required on a CDC 6400 digital computer for the solution of each case involving turbulent flow.

1. INTRODUCTION

THE widespread application of the ESR Process has stimulated considerable interest in the mathematical modeling of these systems. A good review of recent work is available in a paper by Mitchell *et al*,[1] which may be summarized by stating that while very useful work has been done by Pridgeon, Mitchell, Elliott and others on modeling the pool profiles by fitting coefficients to Fourier's equation, no predictive relationships have been developed for the fluid flow fields in the slag and the metal pool. Complementing some very elegant physical modeling work Campbell[2] cited some relationships between current and melt velocities, however, these could not be used even for predicting the orders of magnitude involved.

Notwithstanding the fact that the prediction of the melt velocities in the ESR process is a difficult task because it requires the solution of Maxwell's equations together with the turbulent Navier-Stokes equations, such work is thought to be very worthwhile, for a number of reasons, enumerated in the following.

The development of a predictive thermal model of the process (*e.g.* the computation of the pool profiles for various geometries and current inputs) is not possible without the knowledge of the spatially distributed heat generation in the slag and the convective heat transfer processes in the pool, which in turn depend on the fluid flow. It is stressed in this context that the models that are available at present, while very useful, are essentially interpretive, rather than predictive.

Another, equally important, point is that both the refining process and the structure of the ingot produced are critically dependent on the flow fields and turbulence levels in the slag and in the molten metal pool. The profound effect of fluid flow on the morphology of the solid phases formed is readily appreciated as a result of recent work by Flemings,[3] Tsavaras[4] and others on various solidification processes. The work to be described in this paper is part of a continuous effort aimed at the development of a comprehensive, predictive mathematical representation of the ESR process, with the ultimate purpose of establishing predictive relationships between the system geometry, current input, pool profiles and other process variables.

In the present paper we shall present a mathematical formulation, together with some computed results for the electromagnetic force field, turbulence parameters and melt velocities for both laboratory and industrial scale systems, having a somewhat idealized pool geometry, and operated with a direct current.

2. FORMULATION

A detailed technical description of the ESR process is available in the literature. Fig. 1 shows a sketch of an ESR system, the principal components of which are:

a consumable electrode;
a molten slag phase;
a liquid metal pool;
a solidified ingot; and
a water cooled mold.

It is seen that a current (AC or DC) is passed from the electrode through the molten slag and the liquid pool to the ingot. Due to the resultant Joule heating in the slag (which has a much higher electrical resistance than the metal phases) melting of the electrode occurs and the droplets thus formed fall through the slag and accumulate in the metal pool. Because of the water cooling provided in the mold, solidification occurs continuously at the pool-solid interface and the shape of the pool is in fact determined by a dynamic heat and material balance. An

A. H. DILAWARI and J. SZEKELY are Visiting Engineer and Professor of Materials Engineering, respectively, Department of Materials Science and Engineering, Massachusetts Institute of Technology, Cambridge, MA 02139. A. H. Dilawari is presently on leave from Institute of Chemical Engineering and Technology, Punjab University, Lahore-1, Pakistan.

Manuscript submitted August 10, 1976.

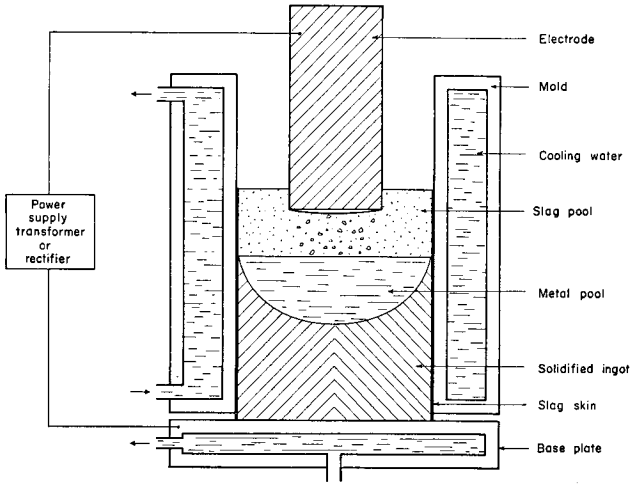

Fig. 1—Schematic sketch of the electroslag remelting process.

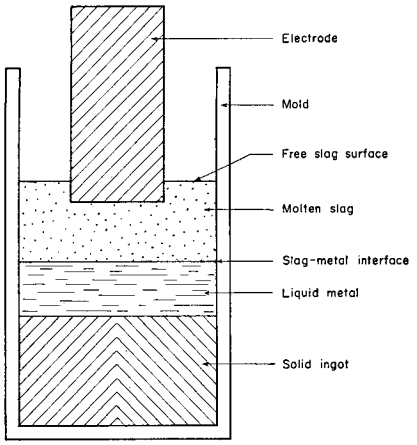

Fig. 2—Physical concept of the process model.

important feature of the process is the fact that a slag skin is formed at the inner surface of the mold, which provides an electrical insulation separating the mold from the molten slag and the liquid pool.

In the development of a model for the process, it has to be recognized that the passage of a spatially nonuniform current from the electrode through the slag and the metal pool, both of which are electric conductors, results in an electromagnetic force field, which in turn generates a fluid flow field both in the slag and in the liquid metal pool.[5] The proper statement of the problem will then require both the definition of this electromagnetic force field and the expression of the appropriate fluid flow equations. Ultimately these equations will have to be coupled with a heat balance representing the spatially nonuniform heat generation in the slag due to Joule heating.

However, in order to make the problem manageable, in the first instance, we shall assume that the liquid pool is defined and concentrate our attention on the electromagnetic and the fluid flow problems only.

The physical concept of the process model is sketched in Fig. 2. It is seen that both the electrode and the liquid metal pool are assumed to have a cylindrical shape; moreover the slag-electrode, slag-pool, and the pool-ingot boundaries are represented by horizontal surfaces. On the basis of published information on large scale systems the shape assumed for the electrode is thought to be reasonable; the shape assumed for the liquid pool is certainly an oversimplification, although this is not thought to have a major effect in the central portion of the pool.

In the statement of the problem the following key assumptions are made:

1) The size of the liquid pool is assumed to be known.

2) Both the slag region and the metal pool are assumed to be isothermal, thus the physical property values are constant in each phase.

3) The effect of metal droplets on the motion of the liquid pool is neglected.

4) Movements of the consumable electrode and of the pool-ingot boundary are assumed negligible.

5) The effect of the electromagnetic force field in damping the turbulent fluctuations is neglected, in the absence of satisfactory methods for doing so.

6) Cylindrical symmetry.

In general these assumptions were dictated by the primary objective of the present work, to assess the effect of the electromagnetic force field on the fluid flow in the slag and the metal phases. This is a first, necessary step in the development of a comprehensive, but rather more complex model in the statement of which many of these assumptions may then be relaxed. More specifically,

1) In order that the size and the shape of the liquid pool be calculated, the thermal energy balance equations would have to be solved. Since this was not attempted at present, the pool size was assumed. In view of numerous pool profile measurements reported in the literature, it is thought that the size of the pool may be estimated with reasonable accuracy.

2) By assuming the slag and the metal pool to be isothermal, the effect of natural convection was neglected. The appropriateness of this assumption can be assessed rigorously only through the solution of the complete set of equations, which include a thermal energy balance. An order of magnitude estimate may, however, be made of the electromagnetic and buoyancy forces acting on the system. As shown in Appendix II, the electromagnetic forces appear to dominate, except in the regions in the vicinity of the walls. This suggests that the effect of natural convection is likely to play a secondary role. A similar observation has been made by Campbell.

3) By comparing the momentum of the metal droplets and that of the circulating metal pool, it may be shown that the stirring effect of the metal droplets is not likely to be great.

4) Assumption (4) above is thought to be reasonable because the movement of the electrode and of the pool-ingot boundary is much slower than the velocities found in the slag and in the metal pool.

5) The appropriateness of Assumption (5) above cannot be assessed without further experimental work.

6) Through the assumption of cylindrical symmetry the effect of external magnetic fields and of the effect of possible eccentricity have been neglected. It is known that external fields may be important[5] in

causing ingot defects. It is thought that the main effect of external fields would be to induce a rotating motion about the geometrical axis of symmetry. This effect was not studied in the present work, because the computational cost of modeling three-dimensional systems would have been prohibitive.

2.1 Fluid Flow Equations

Using vector notation, the equation of continuity is written as:

$$\nabla \cdot \mathbf{V} = 0 \qquad [1]$$

and the equation of motion is given as:

$$\rho(\mathbf{V} \cdot \nabla)\mathbf{V} = -\nabla P + \nabla \cdot \mu_e \nabla \mathbf{V} + \mathbf{F_b} \qquad [2]$$

where

μ_e is the effective viscosity, which is the sum of the laminar and the turbulent contributions. In the solution of a given problem μ_e has to be computed, *e.g.* using a technique described by Spalding.[6]

$\mathbf{F_b}$ is the body force vector, due to the electromagnetic force field, which has to be calculated separately.*

*In general $\mathbf{F_b}$ will include both the buoyancy and the electromagnetic forces; however, in the present case natural convection was not considered.

Equations of the type [1] and [2] have to be written down separately for the slag and the molten metal pool; these two sets of equations are related through boundary conditions, which will be discussed subsequently.

2.2 Calculation of the Body Force

The general expression for the body force field in interacting electric and magnetic fields is available in the texts by Landau and Lifshitz,[7] and Hughes and Young.[8]

It may be shown that for the conditions of interest in this study the body force is given by the following:

$$\mathbf{F_b} = \mathbf{J} \times \mathbf{B} \qquad [3]$$

where

$\mathbf{F_b}$ is the body force in N/m^3,
$\mathbf{J}$ is current density in A/m^2, and
$\mathbf{B}$ is the magnetic flux density in Weber/m^2.

The quantities appearing in Eq. [3] may be evaluated through the solution of Maxwell's equations, which may be written as:

$$\nabla \times \mathbf{E} = -\frac{\partial \mathbf{B}}{\partial t} \qquad [4]$$

$$\nabla \times \mathbf{H} = \mathbf{J} \qquad [5]$$

$$\nabla \cdot \mathbf{H} = 0 \qquad [6]$$

where

$\mathbf{E}$ is the electric field in V/m
$\mathbf{H}$ is the magnetic field intensity in A/m.

Furthermore, we have that:

$$\mathbf{B} = \mu_0 \mathbf{H} \qquad [7]$$

where μ_0 is the magnetic permeability in H/m.

Finally, the current density is given by Ohm's Law

$$\mathbf{J} = \sigma(\mathbf{E} + \mathbf{V} \times \mathbf{B}). \qquad [8]$$

Here again we note that Eqs. [4] to [8] have to be written down separately for the slag and the molten metal pool; these two sets of equations are related through the boundary conditions.

Upon combining Eqs. [4], [5], [7], and [8] through standard manipulation[8] we obtain the following expression:

$$\frac{\partial \mathbf{H}}{\partial t} = \nabla \times (\mathbf{V} \times \mathbf{H}) + \eta \nabla^2 \mathbf{H} \qquad [9]$$

which is the transport equation for the magnetic field, where $\eta = 1/\sigma\mu_0$, which is called the magnetic diffusivity. It may be shown, by putting Eq. [9] into a dimensionless form, that for the conditions normally encountered in ESR, the first term on the right hand side may be neglected*; thus we have:

*The detailed calculations are shown in Appendix I; here we note that in a physical sense the magnetic Reynolds number is small, thus the diffusive transport of the magnetic field dominates over the convective transport.

$$\frac{\partial \mathbf{H}}{\partial t} = \eta \nabla^2 \mathbf{H}. \qquad [10]$$

We note here that Eq. [9] together with

$$\nabla \cdot \mathbf{J} = 0 \qquad [11]$$

and the appropriate boundary conditions defines the electromagnetic force field. It follows that Eqs. [1], [2], [3], [10], and [11] constitute the governing equations, together with the differential equations used for defining the effective viscosity, μ_e.

2.3 The Governing Equations in Cylindrical Coordinates

Eqs. [1], [2], [3], [10], and [11] were given in their general, vectorial form. For cylindrical symmetry, in the r–z coordinate system, sketched in Fig. 3, these equations take the following form:

$$r^2\left[\frac{\partial}{\partial z}\left(\frac{\xi}{r}\frac{\partial \psi}{\partial r}\right) - \frac{\partial}{\partial r}\left(\frac{\xi}{r}\frac{\partial \psi}{\partial z}\right)\right] - \frac{\partial}{\partial z}\left[r^3 \frac{\partial}{\partial z}\left(\mu_e \frac{\xi}{r}\right)\right] - \frac{\partial}{\partial r}\left[r^3 \frac{\partial}{\partial r}\left(\mu_e \frac{\xi}{r}\right) + r^2\left(\frac{\partial F_z}{\partial r} - \frac{\partial F_r}{\partial z}\right)\right] = 0. \qquad [12]$$

(equation of motion)

Here F_z and F_r are the components of the body force field, and ξ and ψ, the vorticity and the stream function are defined in terms of V_z and V_r, the axial and radial velocity components as follows:

$$\xi = \left(\frac{\partial V_r}{\partial z} - \frac{\partial V_z}{\partial r}\right) \qquad [13]$$

$$V_r = -\frac{1}{\rho r}\frac{\partial \psi}{\partial r}; \quad V_z = \frac{1}{\rho r}\left(\frac{\partial \psi}{\partial r}\right) \qquad [14], [15]$$

ξ and ψ are related through

$$\xi + \frac{\partial}{\partial z}\left(\frac{1}{\rho r}\frac{\partial \psi}{\partial z}\right) + \frac{\partial}{\partial r}\left(\frac{1}{\rho r}\frac{\partial \psi}{\partial r}\right) = 0. \qquad [16]$$

We note, moreover, that by working in terms of the

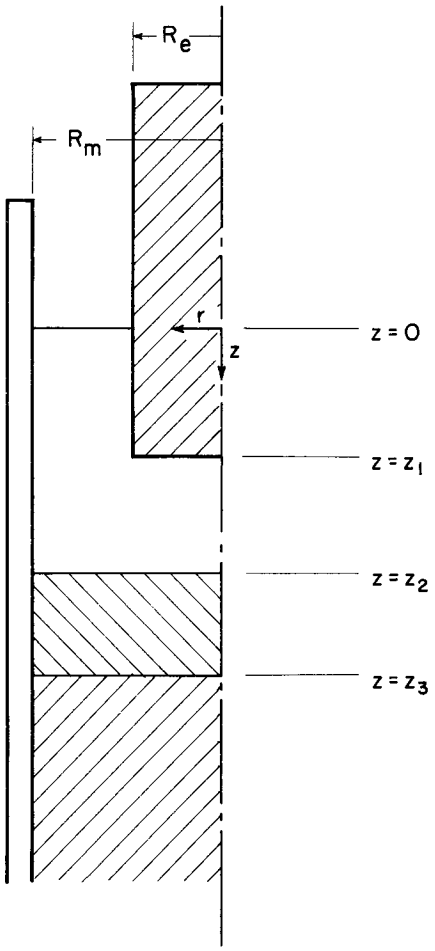

Fig. 3—Sketch of the r-z coordinate system.

stream function the equation of continuity is automatically satisfied.

The transport equation for the magnetic field, originally given as Eq. [10], takes the following form in cylindrical coordinates:

$$\frac{\partial H_\theta}{\partial t} = \eta \left\{ \frac{\partial}{\partial r}\left[\frac{1}{r}\frac{\partial}{\partial r}(rH_\theta)\right] + \frac{\partial}{\partial z}\left[\frac{1}{r}\frac{\partial}{\partial z}(rH_\theta)\right] \right\}. \quad [17]$$

We note here that because of the axial symmetry, $H_z = H_r = 0$ and only H_θ needs to be considered, where H_θ is independent of θ. In the present study the left-hand side of Eq. [17] is set equal to zero. By forming the components of Eq. [5] we have the following:

$$J_r = -\frac{\partial H_\theta}{\partial z} \quad [18]$$

$$J_\theta = 0 \quad [19]$$

and

$$J_z = \frac{1}{r}\frac{\partial}{\partial r}(rH_\theta). \quad [20]$$

It follows from Eqs. [18] to [20] that once $H_\theta(r, z)$ is known, J_r and J_z are readily calculated. From what is said above one can readily define the r- and z- components of the body force field $\mathbf{F_b}$, and thus the body force field term in Eq. [12] is expressed as:

$$r^2\left[\frac{\partial F_z}{\partial r} - \frac{\partial F_r}{\partial z}\right] = 2r\mu_0 H_\theta \frac{\partial H_\theta}{\partial z}. \quad [21]$$

The only remaining task is the definition of μ_e, the effective viscosity. This is readily done, *e.g.*, through the use of Spalding's two equation model, which has been extensively documented.[6,9-11]

2.4 Boundary Conditions

The boundary conditions, the statement of which is required for the definition of the problem, take the following form:

i) Boundary Conditions for the Fluid Flow Equations. The boundary conditions for the fluid flow equations have to express the following physical constraints:

1) Both velocity components are zero at the solid boundaries.

2) Symmetry is observed about the center line, for both the slag phase and the metal pool.

3) The shear stress transmitted through the free surface of the slag is zero.

4) At the slag-metal interface the shear stress and the radial component of the velocity are continuous, while the normal components are zero.

These constraints (1) to (4) above, are readily expressed mathematically and are not reproduced here; the following comments may, however, be appropriate:

The stipulation of zero velocity at the solid surfaces is readily satisfied by setting the stream function equal to a constant, in the present case this constant was chosen as zero.

The criterion for zero shear is readily met by setting the vorticity equal to zero. The expression for zero velocity at the solid boundaries is readily written down in terms of stream function; the corresponding relationship in terms of the vorticity was obtained from the stream field, by expanding ψ in a power series and then using the boundary conditions in terms of ψ, *viz*,

$$\psi = 0 \quad [22]$$

$$\frac{\partial \psi}{\partial r} = 0 \quad [23]$$

$$\frac{\partial \psi}{\partial z} = 0 \quad [24]$$

in conjunction with Eq. [16] at the solid boundary.

At the slag-metal pool interface the values of the stream function are the same in the slag and the metal phases, because the normal velocity components are zero. Moreover, the statement that the shear stress is continuous at the interface may be appropriately manipulated to give the appropriate boundary conditions for the vorticity.

ii) The Electromagnetic Boundary Conditions. The electromagnetic boundary conditions have to express the following physical constraints:

1) The tangential component of the magnetic field intensity, H_θ, is continuous across the boundary between two media, provided there is no surface current at the boundary.

2) The tangential components of the electric field, $\mathbf{E}$, are continuous across the boundaries separating two media.

3) According to Ampere's Law, the line integral of H_θ around the path enclosing the area, through

which the current is flowing, is equal to the enclosed current.

In addition to the above constraints, which express established physical laws, the following assumptions were made, in order to define the problem:

4) In the electrode, corresponding to the horizontal plane,

$$z = 0,\ J_z \gg J_r.$$

5) At the free slag surface, *i.e.*, at $z = 0$, $J_z = 0$.

6) At the interface separating the pool and the ingot, *i.e.*, at

$$z = z_3,\ J_z \gg J_r.$$

7) At the horizontal surface of the electrode (*i.e.*, $z = z_1$), with vertical surface immersed in the slag, covered by a solidified slag crust, $J_{z,s} \gg J_{r,s}$.

The mathematical expression of these constraints takes the following form:

$$H_\theta = 0 \text{ at } r = 0,\ 0 \le z \le z_3 \qquad [25]$$

(symmetry)

$$\left(\frac{\partial H_\theta}{\partial r} + \frac{\partial H_\theta}{r}\right)_e = \frac{\sigma_e}{\sigma_s}\left(\frac{\partial H_\theta}{\partial r} + \frac{H_\theta}{r}\right)_s \text{ at } r = R_e,$$

$$0 \le z \le z_1 \qquad [26]$$

(continuity of electric field, *i.e.*, $E_z|_s = E_z|_e$, using Eq. [8] and Eq. [20]).

$$H_\theta = \frac{I_0}{2\pi R_m} \text{ at } r = R_m,\ 0 \le z \le z_3 \qquad [27]$$

(Ampere's Law)

$$\frac{\partial H_\theta}{\partial z} \simeq 0 \text{ at } z = 0,\ 0 \le r < R_e \qquad [28]$$

(consequence of Assumption (4))

$$\left.\frac{\partial H_\theta}{\partial z}\right|_s = \left(\frac{\sigma_s}{\sigma_e}\right)\left.\frac{\partial H}{\partial z}\right|_e \text{ at } z = z_1,\ 0 \le r \le R_e \qquad [29]$$

(continuity of the electric field)

$$\frac{\partial H_\theta}{\partial z} \simeq 0 \text{ at } z = z_3,\ 0 \le r \le R_m \qquad [30]$$

(consequence of Assumption (6))

and

$$H_\theta(r) = \frac{I_0 r}{2\pi R_m^2} \text{ at } z = 0,\ R_e \le r \le R_m \qquad [31]$$

(consequence of Ampere's Law and Assumption (5))

$$\left.\frac{\partial H_\theta}{\partial z}\right|_s = \left(\frac{\sigma_s}{\sigma_m}\right)\left.\frac{\partial H_\theta}{\partial z}\right|_m \text{ at } z = z_2,\ 0 \le r \le R_m. \qquad [32]$$

(continuity of the electric field)

It is noted that for the magnetic boundary conditions Eqs. [25] to [32] imply that the electrode is in contact with molten slag throughout. If the vertical surface of the electrode, immersed in the slag, is covered by a solidified slag crust, then Eqs. [26] and [29] have to be modified since the solidified slag shell is a poor conductor of electricity.

Thus we have:

$$H_\theta = \frac{I_0}{2\pi R_e} \text{ at } r = R_e,\ 0 \le z \le z_1 \qquad [33]$$

(Ampere's Law)

$$\frac{\partial H_\theta}{\partial z} \simeq 0 \text{ at } z = z_1,\ 0 \le r < R_e. \qquad [34]$$

(consequence of Assumption (7))

Also, Eq. [28] becomes redundant.

3. METHOD OF SOLUTION

From a mathematical viewpoint the solution of the problem required the integration of a set of simultaneous elliptic, differential equations. The governing equations were solved numerically by the successive integration of the governing equations over a finite difference grid, using a CDC 6400 digital computer. The conceptual flow chart of the computational scheme is shown in Fig. 4. The equations describing the electromagnetic force field were solved first using a 21 × 31 grid. The resultant electromagnetic force field was then used to solve the turbulent Navier-Stokes equations, employing a previously described technique.[12] The compilation time was of the order of 15 s and a typical run to describe the turbulent flow field required about 600 to 900 s of computation time.

The computation involved a iterative procedure and here the following convergence criterion was used

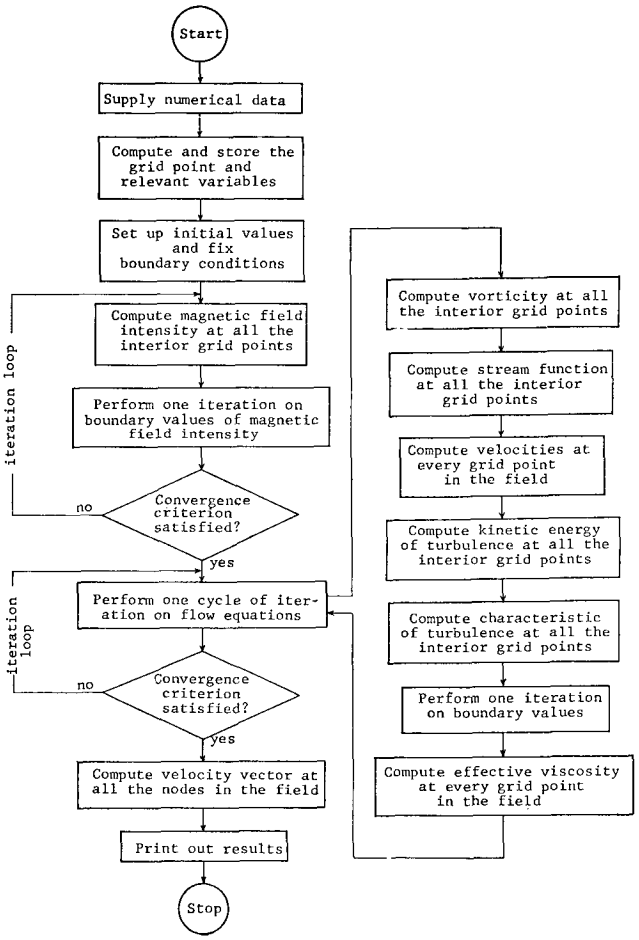

Fig. 4—Simplified schematic flow diagram of the computer program.

$$\left(\frac{\sum_{j=1}^{n} |x_j - x_j^0|}{\sum_{j=1}^{n} |x_j|} \right) < \epsilon \qquad [35]$$

where ϵ equal to 10^{-8} was used for solving electromagnetic field equations and ϵ equal to 10^{-3} for the solution of flow equations.

It is noted that with the number of grid points used, no problems were encountered with the stability of the solution. Trial solutions were generated with both a larger and a smaller number of grid points and it was on that basis that the present arrangement was chosen. It is estimated that the computational error did not exceed about 5 pct, regarding the fluid flow equations; the error was rather less in the computation of the magnetic field equations.

4. COMPUTED RESULTS

In the following Figs. 5 to 15 we shall present a selection of the computed results obtained through the numerical solution of the governing equations described in Section 2.

The principal property values used in the computation are summarized in Tables I and II; Table I refers to conditions in small, laboratory scale installations while the parameters given in Table II are typical of industrial scale systems.

Fig. 5 shows a map of the magnetic field intensity computed for a large scale system, the behavior of a laboratory scale unit is similar, except for an appropriate scaling factor. It is noted that two specific cases have been considered for the purpose of computation,

(*A*) when the vertical walls of the electrode are covered by a solidified slag layer, depicted by the solid line, and

(*B*) when the electrode is not covered by a solidified slag layer, depicted by the broken lines.

It is seen that the resultant magnetic field is markedly modified when a solidified slag crust is formed on the vertical walls of the electrode. The consequence of this difference, in terms of the fluid motion generated, will be discussed subsequently.

Figs. 6 and 7 show the computed velocity fields for the slag and metal phases for a laboratory scale system where the flow is laminar, for Cases (*A*) and (*B*) respectively; the other property values used in the computation have been summarized in Table I.

Inspection of Figs. 6 and 7 shows that the computed velocities in the slag phase are of the order of 5 to 10 cm/s while the melt velocities in the metal pool are substantially smaller, except for the slag-metal interface where the no slip condition has to be observed. It is noted that for Case (*A*), Fig. 6 (the presence of a slag crust over the vertical walls of

Table I. Numerical Values of Parameters Used in the Computation

ρ_m	Liquid-metal density	7.2×10^3 Kg/m^3
ρ_s	Molten-slag density	2.75×10^3 Kg/m^3
μ_m	Liquid-metal viscosity	6.0×10^{-3} Kg/ms
μ_s	Molten-slag viscosity	1.0×10^{-2} Kg/ms
σ_m	Liquid-metal electrical conductivity	7.14×10^5 (ohm-m)$^{-1}$
σ_e	Electrode material electrical conductivity	7.14×10^5 (ohm-m)$^{-1}$
σ_s	Molten-slag electrical conductivity	4.0×10^2 (ohm-m)$^{-1}$
μ_0	Magnetic permeability	1.26×10^{-6} henry/m
I_0	Current	1.8 KA
R_e	Electrode radius	2.5×10^{-2} m
R_m	Mold inside (ingot) radius)	3.5×10^{-2} m
z_1	Electrode immersion in slag	5.0×10^{-2} m
z_2	Molten-slag depth	2.5×10^{-2} m
(z_3-z_2)	Liquid-metal pool depth	5.0×10^{-3} m

Table II. Numerical Values of Parameters Used in the Computation

ρ_m	Liquid-metal density	7.2×10^3 Kg/m^3
ρ_s	Molten-slag density	2.75×10^3 Kg/m^3
μ_m	Liquid-metal viscosity	6.0×10^{-3} Kg/ms
μ_s	Molten-slag viscosity	1.0×10^{-2} Kg/ms
σ_m	Liquid-metal electrical conductivity	7.14×10^5 (ohm-m)$^{-1}$
σ_e	Electrode material electrical conductivity	7.14×10^5 (ohm-m)$^{-1}$
σ_s	Molten-slag electrical conductivity	4.0×10^2 (ohm-m)$^{-1}$
σ_k	Schmidt number of k and w	0.9
σ_w		0.9
μ_0	Magnetic permeability	1.26×10^{-6} henry/m
I_0	Current	18 KA
R_e	Electrode radius	2.5×10^{-1} m
R_m	Mold inside (ingot) radius	3.5×10^{-1} m
z_1	Electrode immersion in slag	5.0×10^{-2} m
z_2	Molten-slag depth	2.5×10^{-1} m
(z_3-z_2)	Liquid-metal pool depth	5.0×10^{-2} m
C_D	Dissipation rate constant	0.09
C_1		3.5
C_2	Constants of the kw model	0.17
C_3		1.04

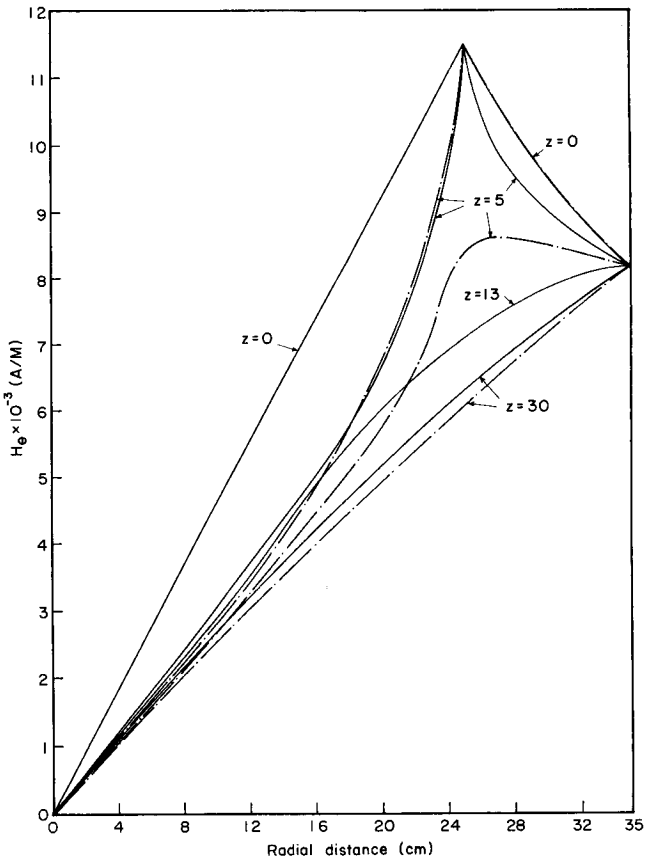

Fig. 5—A map of the computed magnetic field intensity for an industrial scale ESR unit; (—) electrode with solidified slag layer, (—·—) electrode without any solidified slag layer.

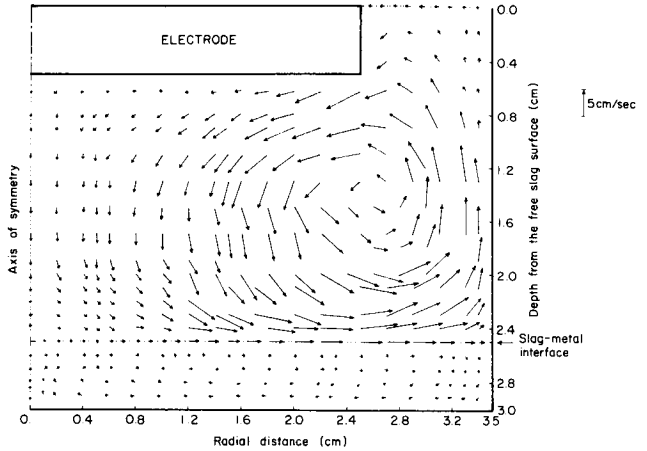

Fig. 6—The computed velocity field in a laboratory scale ESR unit with vertical walls of the electrode covered by a solidified slag layer at a current of 1.8 KA.

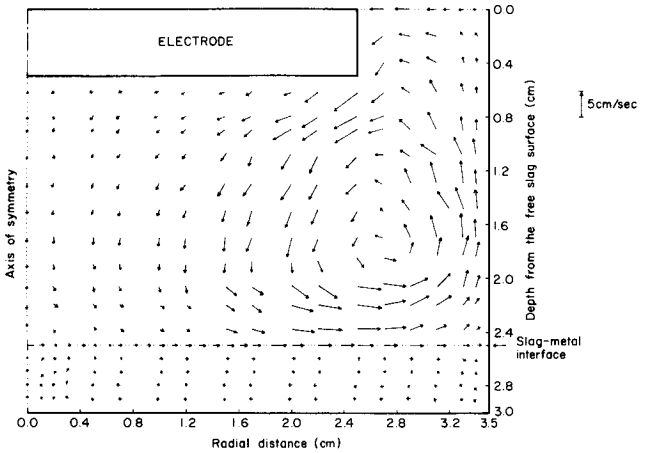

Fig. 7—The computed velocity field in a laboratory scale ESR unit with vertical wall of the electrode not covered by a solidified slag layer at a current of 1.8 KA.

the electrode), the slag velocities appear to be somewhat higher.

This behavior may be explained by the following reasoning. In the ESR system, the electromagnetic force field, which drives the flow, results from the interaction of a spatially nonuniform current with the magnetic field, which is produced by the current itself.

When the vertical walls of the electrode are covered by a solid slag layer, the current density in the slag, below the level of the electrode, is less uniform than for the case when current flows from both the horizontal and the vertical surfaces of the electrode.

Fig. 8 shows the effect of the current on the maximum value of the linear velocity in the slag phase and at the slag-metal interface for a laboratory scale system. It is seen that the velocity appears to be almost a linear function of the current which is a finding of some practical interest.

Figs. 9 and 10 show the computed streamline pattern and the map of the velocity vector computed for an industrial scale system, the property values of which are listed in Table II. Fig. 11 shows a map of the ratio: turbulent viscosity per molecular viscosity, computed for the same conditions, as in Figs. 9 and 10.

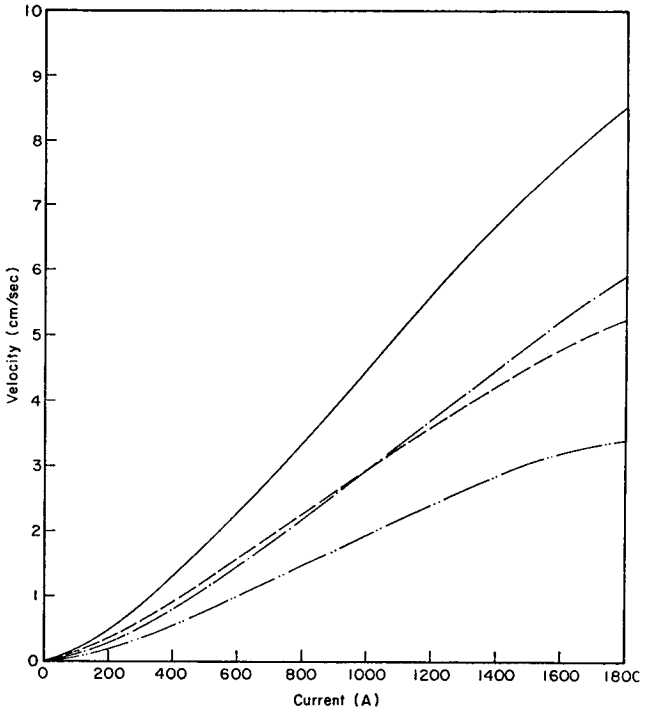

Fig. 8—The effect of current on the maximum value of the linear velocity in the slag phase and at the slag metal interface in a laboratory scale ESR unit; (—) velocity in slag for electrode with solidified slag layer, (---) velocity at the slag-metal interface for electrode with solidified slag layer, (—·—) velocity in slag for electrode without solidified slag layer, (—··—) velocity at the slag-metal interface for electrode without solidified slag layer.

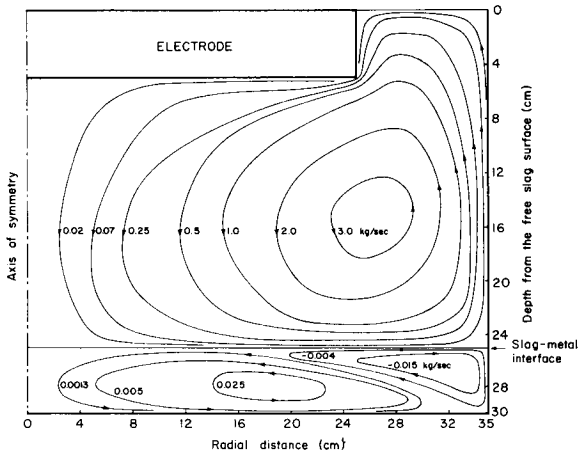

Fig. 9—Computed streamline pattern for an industrial scale ESR system where the electrode is covered with solidified slag layer at a current of 18 KA.

It is noted that while the absolute values of the velocity are quite similar in Figs. 6 and 10, the current density in the laboratory scale unit was about 10 times larger than the corresponding value in the industrial system. For comparable current densities the melt velocities in the laboratory scale system would have been much smaller than in the industrial unit. As indicated in Fig. 8, the ratio of the maximum velocities would have been about 1 : 20.

Inspection of Fig. 11 indicates that the flow is not laminar, although the ratio of the turbulent viscosity to the molecular viscosity is not very large.

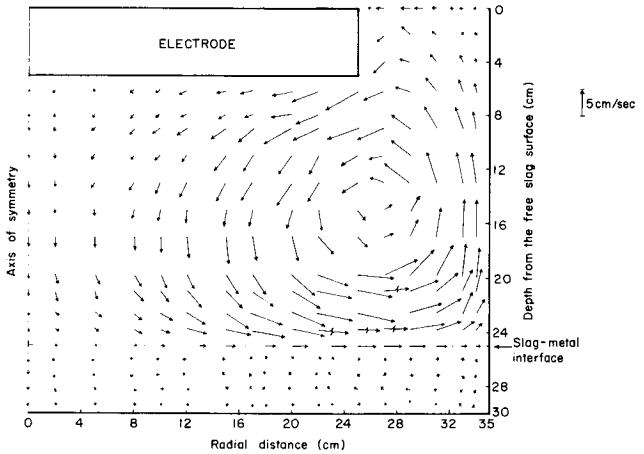

Fig. 10—The computed velocity field in an industrial scale ESR system where the electrode is covered with solidified slag layer at a current of 18 KA.

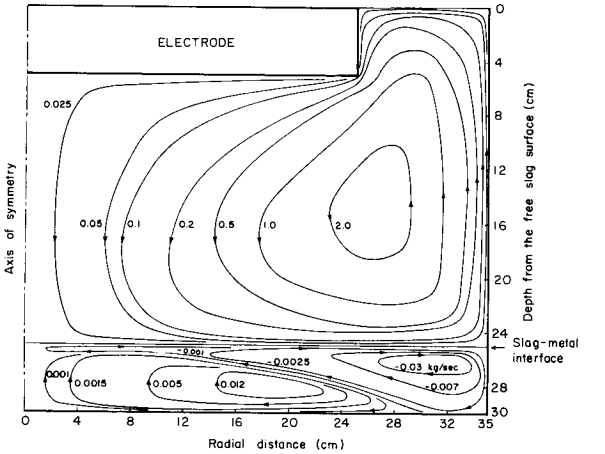

Fig. 12—Computed streamline pattern in an industrial scale ESR system with no solidified slag crust over the vertical walls of the electrode at a current of 18 KA.

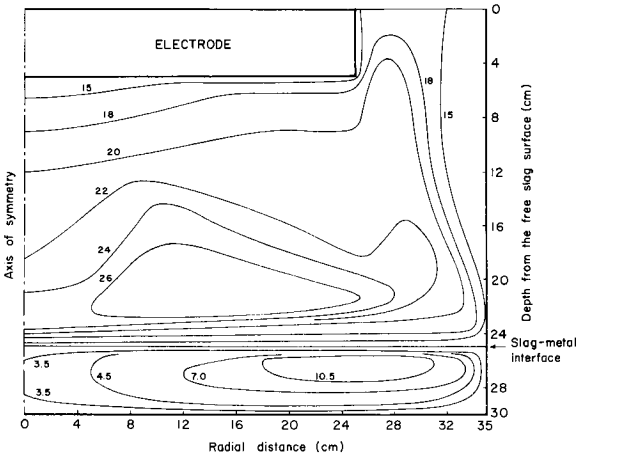

Fig. 11—The computed contours of the ratio: turbulent viscosity per molecular viscosity in an industrial scale ESR system where the electrode is covered with a solidified slag layer at a current of 18 KA.

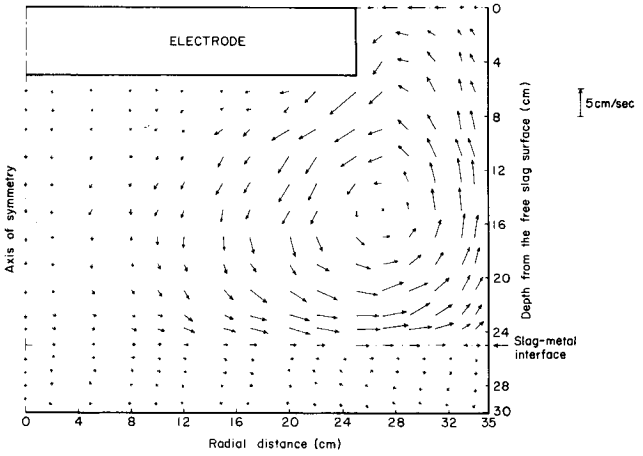

Fig. 13—The computed velocity field in an industrial scale ESR system with no solidified slag crust over the vertical walls of the electrode at a current of 18 KA.

Figs. 12 and 13 show a plot of the streamline pattern and a map of the velocity vector for an industrial scale system and for Case (*B*), that is, when the electrode is not covered by a slag crust. The plot indicates a somewhat lower numerical value of the linear melt velocities. The flow pattern for the metal pool is the result of two opposing forces, namely, the electromagnetic force field, which would tend to produce an anticlockwise circulation pattern and the drag of the circulating slag which would produce a circulation in the opposite direction.

Fig. 14 shows a map of the velocity vector for a case identical to that shown in Fig. 10 but for a threefold increase in the current. It is seen that the threefold increase in the current brings about a corresponding increase in the linear velocity. It follows that the relationship depicted in Fig. 8 for laminar systems appears to hold for turbulent flow fields also.

Fig. 15 shows a map of the ratio: turbulent viscosity per molecular viscosity, for the case depicted in Fig. 14. It is seen upon comparison with Fig. 11, that for the higher current and correspondingly larger body force field, the flow appears to become more turbulent.

5. CONCLUDING REMARKS

Through the statement of Maxwell's equations and the turbulent Navier-Stokes equations, a mathematical representation is proposed for the flow field in the slag region and in the molten metal pool of ESR systems. In the statement of the problem the heat transfer effects were not taken into consideration and a somewhat idealized geometry has been assumed for the metal phase. Otherwise the statement of the problem is thought to be quite rigorous, except for the fact that the possible damping effect of the electromagnetic force field on the turbulent flow field was not taken into consideration (because no rational basis exists at present for doing this).

Through the numerical solution of the governing equations, the flow patterns, velocity fields and turbulence parameters were computed for both laboratory scale and industrial scale systems for typical operating conditions. While the computed results were presented for DC operation only, preliminary computed results indicate qualitatively very similar behavior for AC systems.[13] More specifically, the velocity field in the slag is not affected, whether AC or DC is being used; however, because of the skin ef-

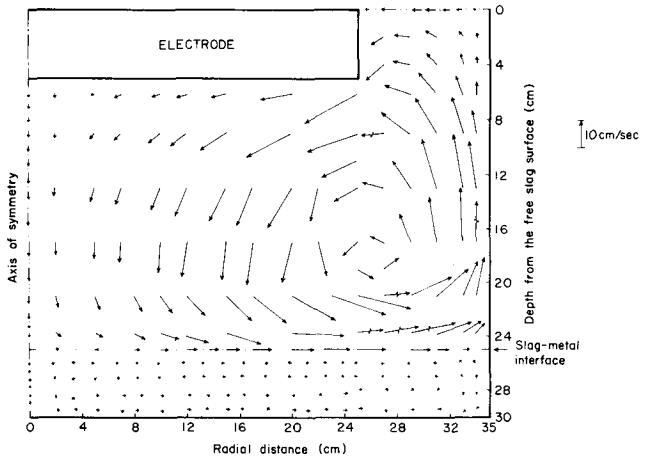

Fig. 14—The computed velocity field in an industrial scale ESR system where the electrode is covered with solidified slag layer at a current of 54 KA.

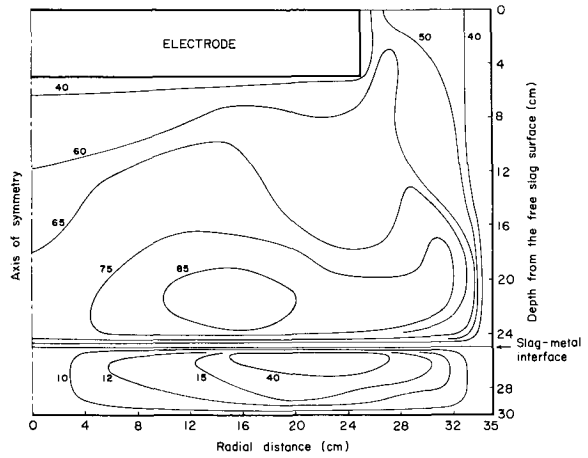

Fig. 15—The computed contours of the ratio: turbulent viscosity per molecular viscosity in an industrial scale ESR system where the electrode is covered with solidified slag layer at a current of 54 KA.

fect, somewhat higher pool velocities result when AC is being employed.

It is thought that this study breaks entirely new ground because this appears to be the first published paper where melt velocities are predicted from first principles in ESR systems. At present there are no quantitative measurements against which the predictions of this model may be tested. The following points may, however, be noteworthy.

The flow patterns predicted for the slag phase for a laboratory scale unit, are consistent with the observations of Campbell for a transparent system.

In a recent mathematical model of the pool profiles in ESR systems, Elliott and Maulvault[14] proposed that by assigning an "effective thermal conductivity" to the pool ranging from 2 to 5 times the atomic value, reasonable agreement may be produced between measurements and predictions. This postulate is consistent with the findings reported here because the relatively small enhancement in conductivity is attributable to (laminar) convective circulation rather than to strong turbulence.

Work is continuing with the objective of incorporating heat transfer phenomena and thus developing predictive relationships for the pool profiles and electrode profiles. This step is the necessary prerequisite of devising scale-up and design criteria for ESR systems, based on the fundamentals. Logical further developments would involve the predictions of droplet trajectories through the slag and hence the refining rates, together with the establishment of relationships between the operating conditions and the product morphology.

APPENDIX I

Let us prove the validity of the approximation made in the text in the derivation of the expressions for the magnetic and electric fields. In a moving medium, the exact expression for the magnetic field equation is given by Eq. [9] rather than [10] adopted for computation.

Eq. [9] may be written in a dimensionless form by defining the following quantities.

$$\mathbf{H}^* = \mathbf{H}/H_0;\ t^* = t/t_0 = tV_0/L_0;$$

$$\mathbf{V}^* = \mathbf{V}/V_0;\ \nabla^* = L_0 \cdot \nabla;$$

$$\nabla^{*2} = L_0^2 \cdot \nabla^2. \qquad [A\text{-}1]$$

In the above definitions subscript 0 refers to a characteristic value. Using the definitions contained in [A-1], Eq. [9] may be expressed in the following form:

$$\frac{\mathbf{H}^*}{t} = \frac{1}{R_M}(\nabla^{*2}\mathbf{H}^*) + \nabla^* \times (\mathbf{V}^* \times \mathbf{H}^*). \qquad [A\text{-}2]$$

where R_M ($= V_0 L_0 \sigma \mu_0$) is called the magnetic Reynolds number, which is a measure of the ratio of the magnetic convection to magnetic diffusion.

For the problem under study, in the slag phase, one may choose the following values for the quantity involved in the definition of R_M, *i.e.*,

$$L_0 = 1 \text{ m}$$
$$V_0 = 1 \text{ m/s}$$
$$\sigma = 4 \times 10^2 \text{ (ohm-m)}^{-1} \qquad [A\text{-}3]$$
$$\mu_0 = 1.26 \times 10^{-6} \text{ henry/m}$$

which result in a value of 8.04×10^{-4} for the magnetic Reynolds number in the slag phase. Since R_M is much smaller than unity the convection term (second term on the rhs of Eq. [A-2]) may be dropped without any loss of accuracy in results.

In the metal pool, however, because of the higher electrical conductivity of the material, one may expect a value of R_M greater than unity. As a first approximation, the convection term in Eq. [9] was dropped while computing the magnetic force field in the metal pool of a typically large DC operated ESR unit. The computed force field gave rise to velocities which were much smaller than the characteristic velocity V_0, chosen for slag phase. Furthermore, the dimension of the metal pool is quite small compared to the characteristic length used for slag phase calculations. For the problem under question, in the metal pool, one may choose the following values for the quantities involved in the definition of R_M, *i.e.*,

$L_0 = 0.5$ m

$V_0 = 0.1$ m

$\sigma = 7.14 \times 10^5$ (ohm-m)$^{-1}$

$\mu_0 = 1.26 \times 10^{-6}$ henry/m [A-4]

which result in value of 4.45×10^{-2} for the magnetic Reynolds number in the metal phase; this is again much smaller than unity. Therefore, the convection term in the magnetic field equation (Eq. [A-2]) may also be dropped for magnetic force field computation in the metal pool without any loss of accuracy in results.

APPENDIX II

In order to assess the relative importance of thermally driven natural convection and the electromagnetically driven flow, let us write the equation of motion in a form such that the body force field includes both these effects. It may be shown that under these conditions the vorticity transport equation, *i.e.*, Eq. [12] in the text, takes the following form:

$$r^2\left[\frac{\partial}{\partial z}\left(\frac{\xi}{r}\frac{\partial \psi}{\partial r}\right) - \frac{\partial}{\partial r}\left(\frac{\xi}{r}\frac{\partial \psi}{\partial z}\right)\right] - \frac{\partial}{\partial z}\left[r^3\frac{\partial}{\partial z}\left(\mu_e\frac{\xi}{r}\right)\right] - \frac{\partial}{\partial r}\left[r^3\frac{\partial}{\partial r}\left(\mu_e\frac{\xi}{r}\right)\right] - r\left[2\mu_0 H_\theta J_r + r\rho_0\beta g\left(\frac{\partial T}{\partial r}\right)\right] = 0. \quad [A-5]$$

Thus we have to compare the terms $2\mu_0 H_\theta J_r$ and $r\rho_0\beta g(\partial T/\partial r)$. The quantity $2\mu_0 H_\theta J_r$ has been computed and was found to vary from about 2.8×10^3 N/m^3 at the electrode to zero, both at the centerline and at the mold wall.

The temperature gradients in the system cannot be predicted a priori without the solution of the energy balance equation. It has been noted, however, both by Campbell[2] and by Mitchell[15] that the temperature gradients in ESR systems are largely confined to the wall regions. Since the natural convection results from temperature gradients and the electromagnetic force field has finite nonzero values over much of the domain, it may be reasonable to assume that natural convection does not play a dominant role in determining the flow field. It would be desirable, however, to obtain independent verification of this assumption; such work is planned for the near future.

LIST OF SYMBOLS

$\mathbf{B}$	magnetic field,
C_D	dissipation rate constant,
C_1, C_2, C_3	constants of "two-equation model" of turbulence,
$\mathbf{E}$	electric field,
$\mathbf{F}_b, F_r, F_\theta, F_z$	body force vector and its components in r-, θ-, z-direction,
$\mathbf{H}, H_r, H_\theta, H_z$	magnetic field intensity and its components,
$\mathbf{J}, J_r, J_\theta, J_z$	current density and its components,
k	kinetic energy of turbulence,
L_0	characteristic length,
r	radial coordinate,
R_e	radius of the electrode,
R_m	inside radius of the mold,
R_M	magnetic Reynolds number,
t	time,
$\mathbf{V}, V_r, V_z$	velocity vector and its components in r- and z-directions,
V_0	characteristic velocity,
w	characteristic property of turbulence,
x_j	values of the dependent variable at grid point j at Nth, iteration,
x_j^0	values of the dependent variable at grid point j at $(n-1)$, iteration,
z	axial coordinate,
z_1	length of electrode immersed in slag phase,
z_2	depth of slag phase,
z_3	total depth of the slag and the metal pool.

GREEK SYMBOLS

η	magnetic diffusivity,
μ, μ_t, μ_e,	molecular, turbulent and effective viscosity,
μ_0	magnetic permeability,
ξ	θ-component of the vorticity vector,
ρ	density,
$\sigma_e, \sigma_s, \sigma_m$	electrical conductivity of electrode, slag and molten metal,
σ_k, σ_w	Schmidt number of k and w,
ψ	stream function,
ϵ	convergence criterion.

ACKNOWLEDGMENTS

The authors wish to thank the National Science Foundation, for support of this investigation, under Grant No. DMR7509476. Thanks are also due to Professor C. P. Yu of the State University of New York at Buffalo, for helpful discussions.

REFERENCES

1. A. Mitchell, J. Szekely, and J. F. Elliott: *Proc. Int. Symp. Electro-Slag Remelting*, pp. 3-15, Sheffield, England, 1973.
2. J. Campbell: *J. Metals*, July, 1970, vol. 22, p. 23-35.
3. S. A. Metz and M. C. Flemings: *AFS Trans.*, 1970, vol. 78, p. 453.
4. A. A. Tsavaras: *Proc. Symp. on Continuous Casting*, p. 197, Chicago, AIME, 1973.
5. R. C. Buehl and J. K. McCauley: *Trans. Inst. Voc. Met. Conf.*, 1967, pp. 695-709.
6. D. B. Spalding: *VDI-Forschungsh.*, 1972, vol. 38, no. 549, pp. 5-16.
7. L. D. Landau and E. M. Lifshitz: *Electrodynamics of Continuous Media*, Addison-Wesley, Reading, Mass., 1960.
8. W. F. Hughes and F. J. Young: *The Electromagneto-dynamics of Fluids*, John Wiley, New York, N.Y., 1966.
9. J. Szekely and K. Nakanishi: *Met. Trans. B*, 1975, vol. 6B, pp. 245-56.
10. J. Szekely and S. Asai: *Trans. Iron Steel Inst. Jap.*, 1975, vol. 15, pp. 270-75.
11. J. Szekely and S. Asai: *Ibid*, 1975, vol. 15, pp. 276-85.
12. A. D. Gosman, W. M. Pun, A. K. Runchal, D. B. Spalding, and M. Wolfshtein: *Heat and Mass Transfer in Recirculating Flow*, Academic Press, London and New York, 1969.
13. J. Szekely and A. H. Dilawari: *Proc. 5th Int. Symp. on Vacuum Metallurgy and Electroslag Remelting Process*, Munich, 1976 (in press).
14. J. F. Elliott and M. A. Maulvault: *Elec. Furnace Conf. Proc.*, AIME, 1970, vol. 28, p. 13.
15. A. Mitchell and S. Joshi: *Met. Trans.*, 1971, vol. 2, pp. 449-55.